Journal of Alloys and Compounds 488 (2009) 134–137

Contents lists available at ScienceDirect

Journal of Alloys and Compounds

journal homepage: www.elsevier.com/locate/jallcom

The structure and mechanical properties of Fe_3Al–30 vol.% Al_2O_3 nanocomposite

M. Khodaei[a,b,*], M.H. Enayati[a], F. Karimzadeh[a]

[a] Department of Materials Engineering, Isfahan University of Technology, Isfahan 84156-83111, Iran
[b] School of Metallurgy and Materials Engineering, University College of Engineering, University of Tehran, Tehran 11155-4563, Iran

ARTICLE INFO

Article history:
Received 4 August 2009
Received in revised form 31 August 2009
Accepted 1 September 2009
Available online 8 September 2009

Keywords:
Nanostructured materials
Mechanochemical processing
Sintering
Composite materials
Mechanical properties

ABSTRACT

Fe_3Al–30 vol.% Al_2O_3 nanocomposite powder was fabricated via two routes. The first route involved the ball milling of Fe_2O_3–Al–Fe powder mixtures to produce in situ Al_2O_3 nanoparticles in Fe_3Al matrix via mechanochemical reaction of Fe_2O_3 and Al. In the second route, Fe_3Al–Al_2O_3 nanocomposite was prepared by ex situ addition of Al_2O_3 nanopowder to Fe–Al powder mixture followed by ball milling. The prepared powders were subsequently consolidated using cold pressing and sintering. The phase analysis, morphology and microstructure of samples were studied by X-ray diffractometry and scanning electron microscopy. Mechanical properties of consolidated powders were determined using hardness test and flexural strength measurements using three-point flexure test at room temperature. The results showed that the Fe_3Al–Al_2O_3 produced via the first route had a significantly improved microstructure and mechanical characteristics in comparison with material obtained via the second route as well as some other techniques.

1. Introduction

Iron aluminides based on Fe_3Al intermetallic compound possess a combination of attractive physical, thermal and mechanical properties including low density, high tensile strength, good oxidation, corrosion, and sulfidation resistance. These properties along with low cost make Fe_3Al based intermetallic potentially useful for structural and coating applications [1].

Two major problems that restrict the application of Fe_3Al intermetallic compound are poor low-temperature ductility and inadequate high-temperature creep resistance. The high-temperature strength of Fe_3Al can be improved by incorporation of ceramic particles, as reinforcements, into the matrix [2]. Originally, reinforcement phase can be introduced in the matrix by two routs namely ex situ addition of reinforcement particles and in situ formation of reinforcement phase via a displacement reaction; $MO + R \rightarrow M + RO$. The later route can be done by mechanochemical process which has an advantage over other fabrication route because of its capability of producing chemical compatible phase as well as nanosized structure with high uniformity [3]. Several mechanochemically synthesized nanocomposites such as NiAl–Al_2O_3 [4], Al_2O_3–Mo [5], Cu–Al_2O_3 [6], etc. were previously reported.

Thermodynamic considerations of reaction between Fe_3Al and different ceramics revealed that Fe_3Al and Al_2O_3 have better adopting characteristics as there is no interface phase between them [7]. Subramanaian et al. [8,9] reported that ceramic particle, such as alumina, could improve the high temperature strength of Fe_3Al matrix without compromising its oxidation resistance.

In our previous works the modality and mechanism of Fe_2O_3 and Al reaction during ball milling to produce Fe_3Al–Al_2O_3 were discussed based on theoretical adiabatic temperature, T_{ad} [10,11]. The aim of the present work was to investigate the effect of fabrication rout of Fe_3Al–Al_2O_3 nanocomposite on microstructure and room temperature mechanical properties of consolidated parts.

2. Experimental

The raw materials were Fe_2O_3 (particle size <5 μm, 99.99% purity, Merck, Germany), Fe (particle size <300 μm, 99.5% purity, Iran Powder Metallurgy Co., Iran), Al (particle size <100 μm, 99.5% purity, Khorasan Powder Metallurgy Co., Iran), and nanosized Al_2O_3 (particle size <100 nm, 99.98% purity, Johnson Matthey Co., USA) powders. Ball milling of powder mixtures was performed in a Spex 8000 type ball mill. The composition of powder mixtures is listed in Table 1. A total of 7 g powder (ball-to-powder weight ratio 5:1) without any process control agent was milled under argon atmosphere. The milling media were hardened chromium steel consisted of five 12-mm diameter balls confined in a 75-ml volume vial.

The milled powder was uniaxially cold pressed into 16 mm diameter and 3 mm thickness pellets at a pressure of 250 MPa. The green pellets were then sintered in vacuum (10^{-2} torr) using VAS electrical resistance furnace for 1 h at 1400 °C.

The phase transformations occurred during ball milling and subsequent sintering were investigated by X-ray diffractometry (XRD) using a Philips X'PERT MPD diffractometer with CuK_α radiation ($\lambda = 0.15418$ nm). Crystallite size and mean lattice strain of specimens were calculated from XRD patterns using the Williamson–Hall method [12]. Morphology of powder particles and microstructure

* Corresponding author at: School of Metallurgy and Materials Engineering, University College of Engineering, University of Tehran, Tehran 11155-4563, Iran. Tel.: +98 21 82084149; fax: +98 21 88010879.
E-mail addresses: mehdi.khodaii@gmail.com, khodaei@ut.ac.ir (M. Khodaei).

0925-8388/$ – see front matter © 2009 Elsevier B.V. All rights reserved.
doi:10.1016/j.jallcom.2009.09.005

Table 1
Composition of prepared samples.

Designation	Starting composition (wt.%)				Final composition
	Fe	Al	Fe_2O_3	Al_2O_3	
ID1	46.6	21.7	31.7	0	Fe_3Al–30 vol.% Al_2O_3
ID2	68.7	11.1	0	20.2	Fe_3Al–30 vol.% Al_2O_3
ID3	86.2	13.8	0	0	Fe_3Al

of sintered specimen were observed by scanning electron microscopy (SEM) in a Philips XL30 microscope with an energy dispersive spectrometer (EDS) attachment.

Hardness of sintered samples (the average of 15 indentations) was determined using a Leitz microhardness tester with a Vicker's indentor at a load of 100 g. Flexural strength of sintered samples was measured using three-point flexure test according to the ASTM B312 standard. Dense bars were cut from the sintered pellets with a diamond saw and then ground and polished into 3 mm × 5 mm × 15 mm specimens. Three-point flexure tests were carried out at room temperature with a span of 10 mm and cross-head speed of 10 μm/s. The fracture strength of consolidated samples (the average of three tests) was calculated using $S = 3PL/2t^2w$ relation where S (MPa) is flexural fracture strength, P (N) is the force required to rupture, L (mm) is the length of the span of fixture, w (mm) is the wide of specimen, and t (mm) is the thickness of specimen.

3. Results and discussion

The details of Fe_3Al–30 vol.% Al_2O_3 formation during ball milling of Fe_2O_3–Al–Fe powder mixture (ID1) are given elsewhere [11]. Microstructural observations, phase analyses, and thermodynamic consideration based on T_{ad} of mechanochemical reaction of Fe_2O_3 + Al + Fe powder mixture revealed [11] that the reaction occurs in a gradual way to produce Fe_3Al–30 vol.% Al_2O_3. XRD pattern of ID1 powder mixture after 20 h of milling time, Fig. 1(a), included only the Fe_3Al peaks. The absence of diffraction peaks of Al_2O_3 phase appeared to be due to the poor crystallization and/or the nanometer sized of Al_2O_3 phase. Crystallite size of Fe_3Al phase for ID1 sample after 20 h of milling time was 40 nm (Table 2).

Fe_3Al–30 vol.% Al_2O_3 was also fabricated by ball milling of Fe–Al–nanosized Al_2O_3 powder mixture (ID2). As shown in Fig. 2(a), after 20 h of ball milling the structure of ID2 sample only consisted of Fe_3Al intermetallic compound similar to ID1 sample. The diffraction peaks of Al_2O_3 phase were absent on the XRD pattern of ID2 sample. As shown in Table 2, the crystallite size of Fe_3Al phase for ID2 sample after 20 h of milling was 25 nm which is smaller than 40 nm measured for ID1 sample after the same milling time. For comparison reason the corresponding data for single phase Fe_3Al (ID3) prepared by ball milling of Fe and Al powder mixture [11] are included in Table 2.

SEM micrographs of ID1 and ID2 powders after 20 h of milling time are shown in Fig. 3(a) and (b), respectively. Both ID1 and ID2

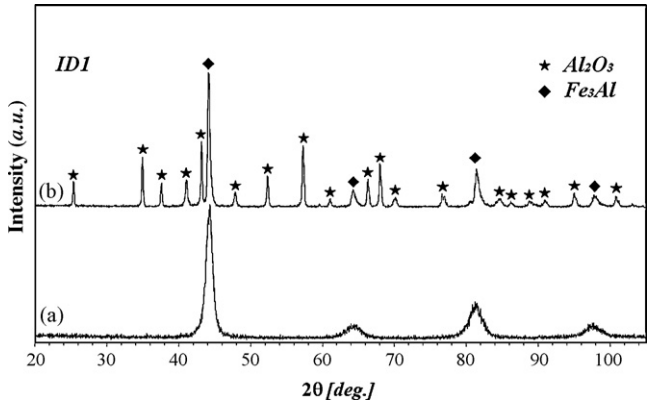

Fig. 1. XRD patterns of Fe_2O_3–Al–Fe powder mixture (ID1): (a) after 20 h of milling time and (b) after 20 h of milling time + sintering for 1 h at 1400 °C.

Table 2
Crystallite size, D, and mean lattice strain, ε, of phases at different stages: (I) 20 h ball milling and (II) 20 h ball milling + 1 h sintering at 1400 °C.

	Process I		Process II	
	Fe_3Al	Al_2O_3	Fe_3Al	Al_2O_3
ID1				
D (nm)	40	–	115	69
ε (%)	1.15	–	0.59	0.19
ID2				
D (nm)	25	–	86	66
ε (%)	1.21	–	0.69	0.18
ID3				
D (nm)	46	–	165	–
ε (%)	1.23	–	0.48	–

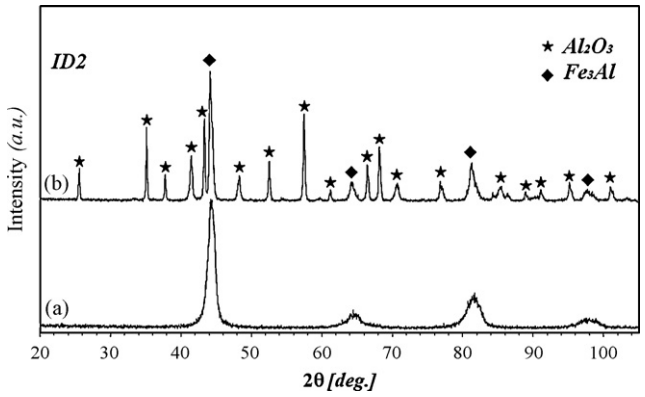

Fig. 2. XRD patterns of Fe–Al–Al_2O_3 powder mixture (ID2): (a) after 20 h of milling time and (b) after 20 h of milling time + sintering for 1 h at 1400 °C.

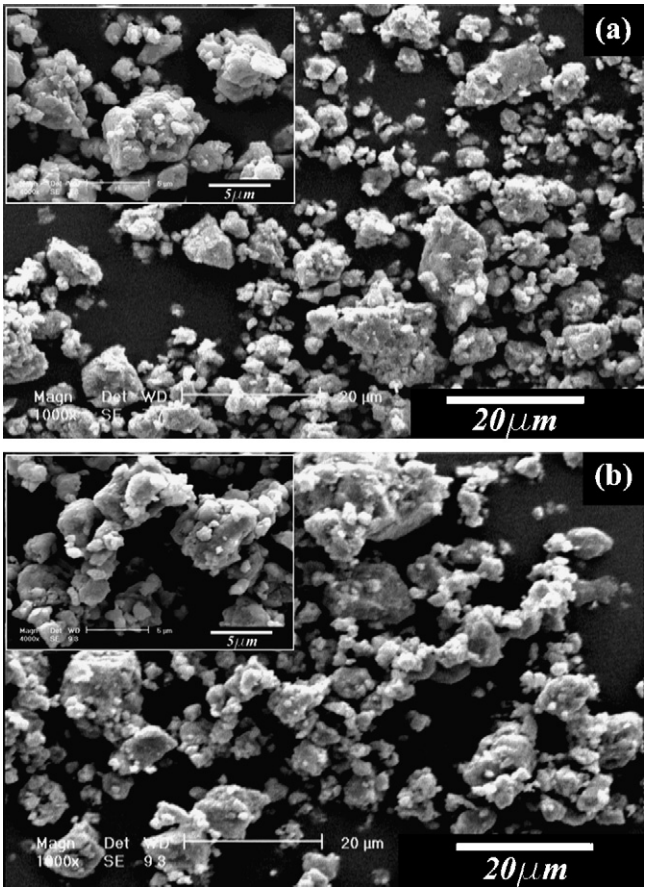

Fig. 3. SEM micrograph of ID1 (a) and ID2 (b) powders after 20 h milling time at different magnifications.

powder particles were irregular in shape with an average size of about 10 μm.

To study the sintering behavior, ID1, ID2, and ID3 powders after 20 h of milling time were cold pressed and then sintered at 1400 °C for 1 h. No swelling and exudation were observed for the ID1 and ID2 pellets, whereas, ID3 sample, which included no Al_2O_3 particles exhibited swelling.

XRD analysis of consolidated samples was performed to determine the crystallite size and structural changes of ID1 and ID2 powders after sintering. XRD patterns of ID1 and ID2 samples after sintering are given in Figs. 1(b) and 2(b), respectively. As can be seen, XRD peaks of α-Al_2O_3 phase are appeared after sintering for both samples. Also, XRD pattern suggests that the disordered structure of Fe_3Al remains unchanged after sintering. The increase in intensity of XRD peaks along with the decrease in their width after sintering are caused by lattice strain recovery and crystallite growth of ball milled powder (Table 2). The Al_2O_3 crystallite size for both ID1 and ID2 samples had similar value of about 65 nm. The crystallite size of Al_2O_3 nanopowder in ID2 samples before sintering was calculated by Scherrer's formula to be about 10 nm. The remarkable increase in crystallite size during sintering could be avoided by using advanced consolidation techniques such as spark plasma sintering (SPS).

Cross-sectional SEM micrographs of the ID1 and ID2 sintered sample are shown in Fig. 4. The dark and bright regions are Al_2O_3 and Fe_3Al phases, respectively, as analyzed by EDS technique. The distribution of Fe_3Al and Al_2O_3 phases in ID2 is not homogeneous whereas for ID1 sample which involved in situ formation of Al_2O_3 by mechanochemical process, a uniform distribution of Al_2O_3 is achieved. Moreover, the microstructure of ID1 sample is finer than that obtained for ID2 sample and contains lower amount of porosity. Peng et al. [13] also reported that Fe_3Al–Al_2O_3 material fabricated by hot pressing of ball milled Fe_3Al and Al_2O_3 nanopowder had undesirable microstructure characterized by severe agglomeration of Al_2O_3 particles within the matrix as well as the weak interfacial bonding. The presence of porosity in ID2 sample at the interfacial cohesion of metallic–ceramic phase might be due to the lack of thermodynamic equilibrium between Fe_3Al and Al_2O_3 nanopowder. In contrast to ID2 sample, the in situ formed Al_2O_3 in case of ID1 sample were continuous giving an interconnected network. The Fe_3Al–20 vol.% Al_2O_3 composite produced via reactive sintering of Fe_2O_3 and FeAl powder mixture by pressureless sintering (ID4) [8] and hot pressing (ID5) [9] had a foam-type feature in which the Al_2O_3 phase are formed as rings around the Fe_3Al matrix, probably from a reaction of FeAl and Fe_2O_3 located along the grain boundaries. These results show that the microstructure of Fe_3Al–Al_2O_3 composite produced by mechanochemical process has better characteristics compared to other processing routes.

Evaluation of the mechanical properties of consolidated samples included the determination of hardness and fracture stress by three-point flexure testing at room temperature. These values are given in Table 3. The hardness of ID1 and ID2 samples was considerably higher than that for ID3 and monolithic cast Fe_3Al (ID6) [9], indicating that the presence of Al_2O_3 increases the hardness

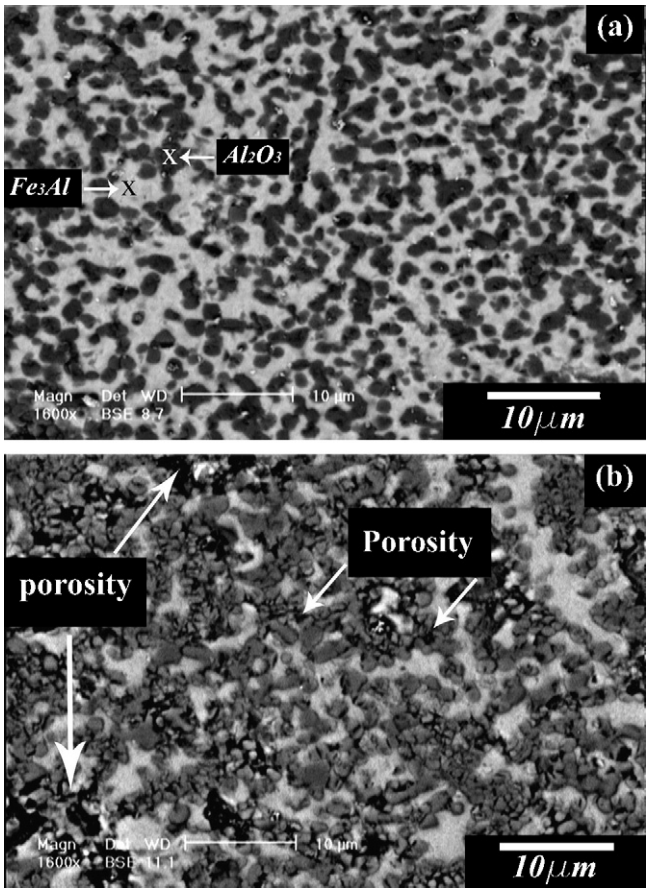

Fig. 4. SEM cross-sectional microstructure of sintered samples: (a) ID1 and (b) ID2. The dark and bright regions are Al_2O_3 and Fe_3Al phases, respectively.

of Fe_3Al phase. The higher hardness value of ID1 and ID2 samples compared to those for ID4 and ID5 samples can be caused by higher fraction of Al_2O_3 phase and its uniform and finer distribution within the matrix.

Fig. 5 compares the room temperature three-point flexure test of ID1 and ID2 samples. The ID2 sample had low fracture stress probably due to the lack of thermodynamic equilibrium and poor interfacial strength between Al_2O_3 nanopowder and Fe_3Al matrix. Also, micro-void presented along the interface of Fe_3Al–Al_2O_3 phases could act as a crack initiation flaws. The ID1 sample, on the other hand, was much stronger. This suggests that the in situ formation of Al_2O_3, during mechanochemical reaction, established strong Fe_3Al–Al_2O_3 interfacial cohesion.

The fracture stress of ID1 sample was higher than that reported for Fe_3Al–20 vol.% Al_2O_3 sample prepared by pressureless sintering (ID4), but is close to the fracture stress of Fe_3Al–20 vol.% Al_2O_3 sample prepared by hot pressing (ID5). It should be noted that the fracture stress of Fe_3Al containing Al_2O_3 phase was lower relative to that for cast monolithic Fe_3Al sample (ID6) due to the presence

Table 3
Vicker's hardness and room temperature three-point fracture stress of prepared samples in comparison with those reported in the literature.

Sample	Composition	Fabrication route of Al_2O_3	Hardness (Hv)	Fracture stress (MPa)	Reference
ID1	Fe_3Al–30 vol.% Al_2O_3	Mechanochemical	538 ± 20	173 ± 9	This work
ID2	Fe_3Al–30 vol.% Al_2O_3	Al_2O_3 nanopowder	490 ± 42	43 ± 6	This work
ID3	Fe_3Al	–	378 ± 19	Not tested	This work
ID4	Fe_3Al–20 vol.% Al_2O_3	Reactive sintering	222[a]	107[a]	[8]
ID5	Fe_3Al–20 vol.% Al_2O_3	Reactive sintering	355 ± 30	184 ± 2	[9]
ID6	Fe_3Al	–	308 ± 5	896[a]	[8,9]

[a] Only one test performed.

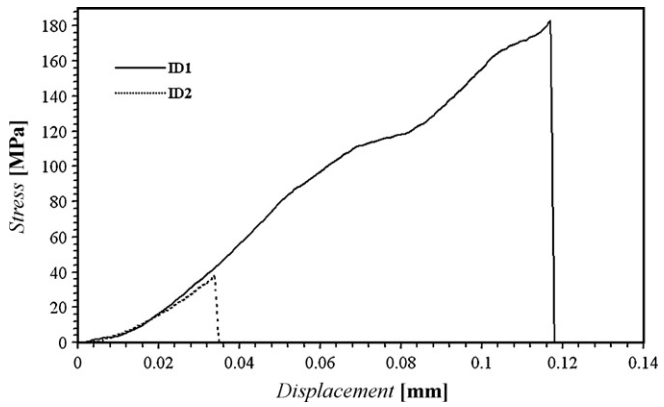

Fig. 5. Room temperature three-point flexure tests of ID1 and ID2 samples.

of Al_2O_3 particles beside the Fe_3Al which can lead to a change in fracture mode [9]. It was not possible to measure the three-point flexure test of ID3 sample because of swelling of sample during sintering. Although increasing the volume fraction of reinforcement generally lead to a decrease in fracture strength of composites [8,9], improving the fracture strength of ID1 sample with 30 vol.% Al_2O_3, compare to the ID4 and ID5 samples, with 20 vol.% Al_2O_3, could be due to the improved distribution of Fe_3Al and Al_2O_3 phases resulting from ball milling process. In reactive sintered samples [8,9], the foam-type feature of Al_2O_3 around the Fe_3Al matrix resulted in the amputation of matrix reducing the fracture strength. Sun and Yeomans [14] proposed that formation of a network microstructure of metallic phase can overcome the poor interfacial cohesion between metallic and ceramic phases. In contrast to the ID4 and ID5 samples, the distribution of Al_2O_3 in Fe_3Al interconnected matrix network lead to the enhancement of fracture strength of ID1 sample.

Further improvement in mechanical properties can be obtained by utilization of external pressure such as hot pressing or HIPing.

4. Conclusion

Fe_3Al–30 vol.% Al_2O_3 nanocomposite powders were fabricated via two routes: ball milling of Fe_2O_3–Al–Fe (ID1) and ball milling of Fe–Al–nanosized Al_2O_3 (ID2).

Microstructure of both samples after sintering consisted of ultrafine (about 2 μm) interconnected Fe_3Al network. Microstructure of ID1 sample, which involved in situ formation of Al_2O_3, was finer and more homogenous than ID2 leading to a higher hardness value of about 538 Hv compared to 490 Hv obtained for ID2 sample. Three-point fracture stress of ID1 sample (173 MPa) was also significantly higher than that (43 MPa) for ID2 sample. The improved mechanical properties of Fe_3Al–Al_2O_3 nanocomposite prepared by mechanochemical route are attributed to the interconnected matrix network resulting from displacement reaction during ball milling process, strong interfacial bonding between Fe_3Al and in situ formed Al_2O_3 phase, and fine and highly uniform distribution of phases within the microstructure.

References

[1] G. Sauthoff, Intermetallics, VCH, Germany, 1995.
[2] D.G. Morris, Intermetallics 6 (1998) 753–758.
[3] C. Suryanarayana, Prog. Mater. Sci. 46 (2001) 1–184.
[4] S.Z. Anvari, M.H. Enayati, F. Karimzadeh, J. Alloys Compd 477 (2009) 178–181.
[5] A. Heidarpour, F. Karimzadeh, M.H. Enayati, J. Alloys Compd 477 (2009) 692–695.
[6] F. Shehata, A. Fathy, M. Abdelhameed, S.F. Moustafa, J. Alloys Compd. 476 (2009) 300–305.
[7] S.L. Draper, D.J. Gaydosh, M.V. Nathal, A.K. Misra, J. Mater. Res. 5 (1990) 1976–1984.
[8] R. Subramanaian, G.C. McKamery, L.R. Buck, J.H. Schneibel, Mater. Sci. Eng. A 239–240 (1997) 640–646.
[9] R. Subramanaian, G.C. McKamery, J.H. Schneilbel, P.M. Menchhofer, Mater. Sci. Eng. A 254 (1998) 119–128.
[10] M. Khodaei, M.H. Enayati, F. Karimzadeh, J. Alloys Compd. 467 (2009) 159–162.
[11] M. Khodaei, M.H. Enayati, F. Karimzadeh, J. Mater. Sci. 43 (2008) 132–138.
[12] G.K. Williamson, W.H. Hall, Acta Metall. 1 (1953) 22–31.
[13] L.M. Peng, H. Li, J.H. Wang, M. Gong, Mater. Lett. 60 (2004) 883–887.
[14] X. Sun, J.A. Yeomans, J. Mater. Sci. 31 (1996) 875–880.